Published in final edited form as:
Anat Histol Embryol. 2011 August ; 40(4): 283–291. doi:10.1111/j.1439-0264.2011.01067.x.

Molecular and structural assessment of alveolar bone during tooth eruption and function in the miniature pig, *Sus scrofa*

Kuang-Dah Yeh[1,2] and **Tracy Popowics**[2,*]
[2] Dept. of Oral Biology, University of Washington, Seattle, WA 98195

Summary

The development of alveolar bone adjacent to the tooth root during tooth eruption is not well understood. This study tested the hypothesis that predominantly woven bone forms adjacent to tooth roots during tooth eruption, but that this immature structure transitions to lamellar bone when the tooth comes into function. Additionally, bone resorption was predicted to play a key role in transitioning immature bone to more mature, load-bearing tissue. Miniature pigs were compared at two occlusal stages, 13 weeks (n=3), corresponding with the mucosal penetration stage of M_1 tooth eruption, and 23 weeks (n=3), corresponding with early occlusion of M^1/M_1. Bone samples for RNA extraction and qRT-PCR analysis were harvested from the diastema and adjacent to M_1 roots on one side. Following euthanasia, bone samples for hematoxylin and eosin and TRAP staining were harvested from these regions on the other side. In contrast to expectations, both erupting and functioning molars had reticular fibrolamellar structure in alveolar bone adjacent to M_1. However, the woven bone matrix in older pigs was thicker and had denser primary osteons. Gene expression data and osteoclast cell counts showed a tendency for more bone resorptive activity near the molars than at distant sites, but no differences between eruptive stages. Thus, although resorption does occur, it is not a primary mechanism in the transition in alveolar bone from eruption to function. Incremental growth of existing woven bone and filling in of primary osteons within the mineralized scaffold generated the fortification necessary to support an erupted and functioning tooth.

Keywords

alveolar bone; tooth eruption; resorption; qRT-PCR

Introduction

Alveolar bone is well known to develop as teeth erupt into function. However, the transitions in bone structure adjacent to the developing tooth root and mechanisms driving these changes are not well understood. Woven bone forms a crypt that surrounds a tooth during development and remodels as the tooth germ grows (Dixon et al., 1997, par Azeredo et al., 2000). With crown formation complete intraosseous tooth eruption begins, corresponding with the resorption of the coronal portion of the alveolar crypt and apposition occurring adjacent to the developing root (Wise et al., 2002, Pilipili et al., 1998, Marks and Cahill, 1986). Lamellar bone apposition and islets of chondroid tissue have been observed underlying the developing tooth root during intraosseous eruption of dog premolars, and woven bone and chondroid tissue filled the space unoccupied by the erupting tooth (Pilipili

[*]Corresponding author: Tracy Popowics, Box 357132, Dept. of Oral Biology, University of Washington, Seattle, WA 98195, Fax: (206) 685-3162, Phone: (206) 221-5350, Popowics@u.washington.edu.
[1]Current address: Hualien Armed Forces General Hospital, Hualien, Taiwan

et al., 1998). Eruption continues as the crown penetrates the oral mucosa and moves toward the occlusal plane. The fully erupted and functional tooth relies on the anchorage of the periodontal ligament (PDL) within the alveolar bone proper (ABP) for immediate occlusal support. Away from the tooth root, cancellous bone fills the interior spaces of the alveolar crest and cortical plates support the outer surface of the dental arches. The architecture of tooth supporting alveolar bone in pigs is further described in a previous study (Yeh and Popowics, 2010) and differs from the structure of the non-supporting bone of the diastema in which the absence of teeth precludes the formation of ABP. The focus of this investigation is how alveolar bone develops adjacent to the tooth root during mucosal penetration and the first application of occlusal load, and thus achieves a structural configuration able to support an occluding tooth.

In particular, we tested the hypotheses that predominantly woven bone forms adjacent to the tooth root during the mucosal penetration stage of tooth eruption, but that this immature structure transitions to lamellar bone during early tooth function. The basis for this hypothesis is that the focused, consistently oriented load that is experienced only after the tooth is in functional occlusion, triggers adaptive remodeling (Yeh et al., 2010, Terespolsky et al., 2002, Saffar et al., 1997). During the mucosal penetration stage, the food bolus may apply low levels of load to the tooth crown through the partially penetrated mucosa, triggering woven bone apposition adjacent to the tooth roots. A similar response may also occur through the flexing of the mandible during chewing, whereby occlusion of adjacent erupted teeth may confer low levels of strain to the alveolar bone of erupting teeth. However, these loads are likely low and relatively unpredictable in orientation. In contrast, when a tooth reaches functional occlusion higher level loads will be transmitted through the crown to the alveolus, requiring the increased osseous support provided by lamellar bone. Frost hypothesized that cortical bone apposition is responsive to strain levels, and that above a threshold microstrain, apposition is activated in order to reduce peak strains (Frost, 1987). This “mechanostat” hypothesis has been supported for the loading of alveolar bone in rats, in that increasing occlusal loads through a bite block or hard diet resulted in increased cortical thickness (Mavropoulos et al., 2004).

In addition to the increased lamellar bone formation corresponding with the onset of tooth function, osteoclasts would have to play a key role in resorbing the woven bone accrued during tooth eruption. Woven bone is a poorly mineralized, highly cellular structure that is likely to be inadequate to withstand occlusal loads, and the early period of occlusion may result in alveolar microcracking. Indeed microcracks have been observed in pig alveolar bone during orthodontic tooth movement (Verna et al., 2004) and are known to stimulate remodeling activity (Burr, 1993, Taylor and Lee, 2003). Such targeted remodeling provides a mechanism for removing inadequate, injured bone structure and replacing it with denser lamellae. Additionally, alveolar bone turnover occurs at a higher rate than other skeletal regions (Huja et al., 2006), suggesting an important role for resorption in alveolar bone adaptation.

This study aims to define the eruptive transition in pig alveolar bone through molecular and structural assessment at the mucosal penetration stage of tooth eruption and at the onset of functional occlusion. Although pig mandibular bone has been studied previously (Powell et al., 1973), most work focused on the cortex and structural studies of large animal alveolar bone has been pursued in dogs (Deguchi et al., 2008, Marks and Cahill, 1986, Huja et al., 2006, Pilipili et al., 1998). Although several studies have addressed gene expression in porcine bone marrow mesenchymal stem cells *in vitro (*Bosch et al., 2006, Zeng et al., 2006, Zou et al., 2004*)*, gene expression in pig alveolar bone remains undescribed *in vivo*. Here, gene expressions associated with the regulation of osteoclast formation, such as the receptor activator of NF-κB ligand (*Rankl*), osteoprotegerin (*Opg*), and colony stimulating factor

(*Csf-1*) were measured in order to assess the role of osteoclast activity in bone adjacent to tooth roots during eruption. Additionally, genes associated with bone formation, such as *Runx2* and *Bsp* were compared between eruptive stages. The bone adjacent to the lower first molar (M_1) was compared with bone from the diastema region (which lacks teeth) in order to establish whether bone structure or gene expression differs in tooth supporting or non-tooth supporting regions.

Material and Methods

Histology

All procedures were humane and approved by the University of Washington Animal Care and Use Committee. Three Hanford miniature pigs were acquired at 13 and 23 weeks of age (n=6; Sinclair Research, St. Louis), corresponding with the mucosal penetration stage of M_1 tooth eruption and early occlusion of M1/M_1 (Figure 1), respectively. Pigs were euthanized by initial anesthetization with isoflurane and subsequent intracardiac injection of pentobarbital. Tissues for histological processing were collected postmortem, fixed in Bouin's solution and decalcified in 8% EDTA or 10% formic acid solution. Decalcified tissues were dehydrated, paraffin embedded and sectioned sagittally at 7μm. Sections including the entire length of the distal root of M_1 were stained with Hematoxylin and Eosin (H&E) and tartrate-resistant acid phosphatase (TRAP) according to the manufacturers' instructions (Sigma kit 387A) and examined using light microscopy. In TRAP stained tissues, the bone posterior to the tooth root was divided into cervical (adjacent to the cementoenamel junction (CEJ)), middle and apical thirds. Two 1 × 1 mm regions were identified, one within the alveolar bone proper (ABP; adjacent to the periodontal ligament) and the other further distal in the cancellous bone (midway between the ABP and the lower second molar (M_2) crypt). Osteoclasts were identified as darkly staining multi-nucleated cells and counted. Non-parametric statistics were used to compare osteoclast cell counts between regions and ages.

Quantitative Real Time Reverse Transcription Polymerase Chain Reaction (qRT-PCR)

Alveolar bone samples from the mandibular diastema and distal M_1 were collected from 3 pigs of each age group (Figure 2). In order to maximize RNA integrity, bone samples were collected from anesthetized animals antemortem with a reciprocal saw (Stryker) and flash frozen in liquid nitrogen. Each sample was ground to a powder using a mortar and pestle and liquid nitrogen. Cellular RNA was isolated from tissues using TRIZOL® Reagent (GIBCO/BRL) and utilized a MagNALyzer® homogenizer (Roche) in order to enhance the separation of protein from cells. An RNeasy Mini kit (Qiagen) was used to remove contaminating DNA from the extracted RNA samples. RNA yields and purity were quantified with a spectrophotometer, and only bone RNA samples showing 260/280 absorbance ratios that were higher than 1.90 were used. Selected samples were also tested to ensure RNA integrity. One RNA sample extracted from 13 week M_1 distal bone (pig 4425) showed degradation and was omitted from further study.

For PCR analysis, cDNA was synthesized using 1.0 μg total RNA with a cDNA synthesis kit (Transcriptor kit, Roche Diagnostic). 2.0 μL of the resulting cDNA product was used per 20 μL reaction in the Roche Lightcycler 480 system. qRT-PCR reactions were carried out with the DNA Master SYBR Green I kit (Roche). Primer sequences were designed from pig or cow partial coding sequences (Table 1) and are intron-spanning to amplify cDNA rather than genomic DNA. In the case of *Runx2* and *Opg*, amplification products generated with cow primers were sequenced to generate partial coding sequences and primers for pig genes

[1]Current address: Hualien Armed Forces General Hospital, Hualien, Taiwan

(GenBank accession # EU668154 and EF543195). A BLAST search of GenBank on the primer sequences was used to confirm specificity, and melting curve analysis of products post-PCR was checked for additional confirmation. Primers were used at a concentration of 0.5 μM. Glyceraldehyde-3-phosphate dehydrogenase (*Gapdh*) served as a housekeeping/reference gene for normalization. As described below, porcine osteoblast DNA was used for qRT-PCR calibration and template DNA was replaced with PCR-grade water as a negative control. The amplification profile used on the Lightcycler was: 95°C /60s; 58°C /60s; 72°C / 60s and 50–55 cycles.

A porcine osteoblast cell culture was used to generate a calibrator DNA for qRT-PCR amplification. The role of the calibrator was to provide a stable ratio of target to reference genes and to normalize all samples within a qRT-PCR run. Pig bone marrow aspirates were obtained from the tibia and mononuclear cells were separated by centrifugation of aspirates through a solution of polysucrose and sodium diatrizoate (Histopaque; density, 1.077; Sigma) according to the protocol of Bosch (2006). Mononuclear cells pipetted from the opaque interface were washed twice in Dulbecco's phosphate-buffered saline (D-PBS) and resuspended in Minimum Essential Medium (MEM) Alpha medium (Invitrogen) supplemented with 10% FBS. Cells were plated on plastic flasks at a density of approximately 500,000 cells/cm^2 and the medium was changed every 24h, washing unattached cells away with the medium change. Adherent fibroblast-like, spindle shape cells grew for 10–14 days, with media replacement every 3rd day. Cells were passaged at 80–90% confluence by trypsinization (0.25% trypsin-EDTA solution) and reseeded at a density of 5000–6000 cells/cm^2 in plastic flasks (Bosch et al., 2006). The cultured porcine mesenchymal cells (pMSCs) were induced to differentiate into osteogenic cells by exposure to media containing ascorbic acid and β-glycerophosphate. The cells' osteoblastic identity was confirmed through staining of the mineralized extracellular matrix with alizarin red. Cells were harvested for RNA extraction and synthesized DNA was used as a calibrator in qRT-PCR experiments.

Each sample was amplified in triplicate for each gene and PCR products were identified with specific melting curves. Gene expression levels were standardized across reactions with corresponding coefficient curves and RelQuant software was used to measure different gene expression levels in different samples. The mean value for triplicate experiments was used to compare samples from different age groups and locations using non-parametric statistical analyses. A p value of less than 0.05 was considered significant.

Results

Bone Structure

The bone distal to the erupting M_1 in the 13 week pigs consisted mainly of reticular fibrolamellar bone adjacent to the tooth roots in all cervical through apical locations (Figure 3A). The mineralized woven bone matrix formed thin trabeculae interspersed with immature primary osteons with large diameter vascular marrow canals. The primary osteons were oriented obliquely throughout the matrix and the vascular canals anastomosed irregularly, agreeing with the category definition for reticular fibrolamellar bone (Francillon-Viellot et al., 1990). In some samples, the most cervical regions were reticular fibro lamellar bone adjacent to the root but laminar bone more distal from the root. Throughout the length of the tooth root, thin trabeculae projected into the periodontal ligament tissue. The diastema region appeared similar to the bone adjacent to the developing tooth root, including mainly fibrolamellar bone (Figure 4A).

In 23-week pigs, the bone distal to the erupted M_1 was also mainly of reticular fibrolamellar structure, however the woven bone matrix was noticeably thicker than in the younger tissue

and canals of the primary osteons were generally smaller (Figure 3B). The overall denser matrix gave the appearance of a less finely reticulated matrix than in the younger tissue. In some cervical locations the alveolar bone was especially dense and contained more longitudinally oriented vascular canals. The woven bone matrix formed a continuous surface or thick trabeculae that extended into the periodontal ligament. The fibrolamellar bone of the diastema showed a similar density to the bone distal to the erupted M_1 with nearly all of the cellular space filled with primary osteons (Figure 4B).

Osteoclast Cell Numbers

TRAP-stained osteoclasts were observed in all alveolar bone proper and cancellous bone regions adjacent to M_1 and did not show marked differences among regions or between age groups (Figure 5). Within alveolar bone proper, osteoclast numbers ranged from 2–12/mm^2 in 13 week specimens and 4–11/mm^2 in 23 week specimens). Osteoclast numbers in the distal location were 0–10/mm^2 at 13 weeks and 2–10/mm^2 at 23 weeks. In comparing bone directly adjacent to the tooth root and bone more distal from the root, osteoclast numbers showed greater similarity in 13 week specimens. In 23 week specimens, osteoclast numbers in bone adjacent to the root tended to be higher than more distal from the root, however, this difference did not reach statistical significance.

The tissue preservation of bone in the diastema region was insufficient to allow osteoclast cell counts; however the bone of the diastema appeared primarily formative. Although osteoclasts were visible in the diastema of both 13 and 23 week pigs, bone surfaces were predominantly smooth with only an occasional appearance of Howship's lacunae.

qRT PCR

Gene expression values were similar between locations and age groups (Table 2). Negative controls produced no amplification of target gene DNAs, whereas the osteoblast DNA calibrator expressed target genes in all cases. When mean values were compared, *Rankl* expression was similar in the M_1 alveolar bone in 13 week and 23 week pigs (0.52 vs. 0.50), and could not be distinguished from *Rankl* expression in the diastema (0.20 vs. 0.39, 13 week and 23 week pigs, respectively). For 4 of the 5 animals available for comparison (all but 5069), however, *Rankl* expression in the M_1 bone was higher than in the diastema, resulting in overall higher mean expression in the M_1 bone of pigs in each age group. *Csf-1* expression was comparable between the M_1 bone samples of 13 and 23 week pigs (means of 0.92 vs. 0.84), as well as in the diastema (means of 0.61 vs. 0.67; 13 and 23 weeks, respectively). As with *Rankl* expression, *Csf-1* expression tended to be higher in each pig, with the exception of pig 5069, in the M_1 distal bone versus the diastema. *Opg* expression was not reliably measured, as triplicate experiments for each sample were highly variable. Means and standard deviations for each sample are reported in Table 2; however, means for each age group were omitted from comparisons. In the case of *Bsp* and *Runx2*, gene expression values were very high, but were also highly variable among individual pigs of each age group, and thus, did not demonstrate differences. When individual animals were examined, these apposition-related genes were higher in M_1 bone than the diastema in 13-week animals, but no consistent trend was seen in the 23-week animals.

Discussion

Contrary to expectations, the alveolar bone supporting fully erupted and functional first molars was not lamellar, but consisted of a dense fibrolamellar matrix that included primary osteons. Younger pigs also showed fibrolamellar structure surrounding the erupting first molars, however, it was less dense and more finely reticulated than the older bone. A previous study of the mandibular cortex in growing pigs demonstrated a plexiform structure

that regionally varied in porosity (Powell et al., 1973), suggesting that this structure may characterize rapidly growing porcine bone. Although the alveolar bone proper is typically described as including lamellar tissue, it was not so in these animals. Nevertheless, the dense fibrolamellar structure observed adjacent to molars in juvenile pigs appears sufficient to support molars in occlusion. Lamellar structure may only occur in these locations with greater maturity or the larger occlusal forces that would correspond with increased body size.

Osteoclast activity was predicted to play a major role in the adaptation of alveolar bone to occlusal loading; however, osteoclast cell counts indicate at most a minor role for resorption in the osseous changes surrounding M_1 tooth roots. Osteoclast numbers were similar adjacent to and distal from the root in 13 week tissues, suggesting a constitutive level of turnover in the alveolar bone during the mucosal penetration stage of M_1 eruption. However, at 23 weeks, although osteoclast numbers were at levels similar to the 13 week bone, adjacent to the erupted molars, away from the root osteoclast numbers appeared to be dropping. This suggests the possibility of an age-related drop in constituitive resorption, while higher levels are maintained for bone anchoring PDL fibers in order to respond to occlusal loads transmitted through the PDL. This suggestion is consistent with previous observations in rat alveoli where resorption plays an active role in modeling of the alveolar bone proper (Saffar et al., 1997, Vignery and Baron, 1980).

The consistent expression of *Rankl* and *Csf-1* in alveolar bone associated with erupting and functioning molars further indicates the presence of constitutive levels of resorption. The membrane of osteoblast/stromal cells expresses RANKL in response to bone resorbing signals, and all phases of osteoclastogenesis depend on the interaction between RANKL and the transmembrane signaling receptor, Rank, present on osteoclast progenitors (Yasuda et al., 1998, Yasuda et al., 1999). The cytokine CSF-1 is necessary for both proliferation and differentiation of osteoclast progenitors at remodeling sites (Katagiri and Takahashi, 2002, Van Wesenbeeck et al., 2002). The expression of *Rankl* and *Csf-1* in porcine alveolar bone demonstrates the involvement of these genes in the promotion of osteoclast formation, but their similar expression levels indicate that peaks in resorption do not accompany the onset of occlusal activity. On the other hand, the *Rankl* gene expression levels distal to M_1 showed a tendency to be higher than the diastema region, suggesting that bone surrounding tooth roots may have a higher turnover than toothless regions of the dental arch. Although osteoclast cell counts were unavailable in the poorly preserved diastema samples, bone surfaces in this region appear primarily formative, corresponding with lower *Rankl* expression in the diastema. Previous studies have shown that increases in *Rankl* expression correspond with increased remodeling (Fazzalari et al., 2001) and occur in fractured bone during repair processes (Kon et al., 2001). Studies of the bone overlying the tooth crown during the earlier intraosseous eruption demonstrate spikes in osteoclast cell numbers and expression of resorption associated genes *Rankl* and *Csf-1* as an intraosseous eruption pathway is formed (Wise et al., 1999, Liu et al., 2005, Wise et al., 2005), but these features decline in basal regions surrounding the developing tooth root in mice at later eruptive stages (Heinrich et al., 2005). Application of excessive orthodontic forces on rat teeth can upregulate *Rankl* expression on the compression side of the alveolar bone (Ogasawara et al., 2004). Furthermore, a hyperocclusion mouse model has demonstrated increased osteoclasts and significant increases in *Rankl* expression in periodontal tissues (Walker et al., 2008). The tendency toward an increase in *Rankl* expression in bone distal to M_1 tooth roots in the present study does not reach the magnitude previously observed during intraosseous eruption or in studies that manipulate the periodontal loads. Therefore, we conclude that although resorption is active in resorbing woven bone surrounding roots, a large-scale removal of inappropriately structured or microfractured alveolar tissue does not accompany the onset of occlusion.

Consistent expression of genes associated with osteogenesis, *Runx2* and *Bsp*, suggests that incremental bone apposition generates the major structural differences in alveolar bone between 13 and 23 week pigs. *Runx2* expression has been identified as a molecular switch stimulating mesenchymal cells to differentiate into osteoblasts and triggering expression of major bone matrix genes (Ducy, 2000, Zhang et al., 2009, Ducy et al., 1997, Komori, 2010), processes which in occur in alveolar bone cells as well as elsewhere (Perinpanayagam et al., 2006). Multiple signal transduction pathways regulate *Runx2* expression, including those involved in mechanotransduction (Franceschi and Xiao, 2003). BSP is thought to nucleate hydroxyapatite at the bone mineralization front (Ogata, 2008) and is strongly expressed in osteocytes and osteoblasts within porcine alveolar bone (Chen et al., 1993). The present study did not detect differences in *Runx2* or *Bsp* expression associated with age or eruptive status, indicating that bone growth or occlusal loading did not upregulate expression. Instead, high expression is probably associated with progressive apposition throughout the entire period of growth and eruption, thickening trabeculae and forming primary osteons within a pre-existing woven bone scaffold.

Although osteoblast gene expression has received much attention through study of *in vitro* cell cultures, little data are available on *in vivo* expression patterns, particularly in response to changes in functional conditions. The regulation of *Rankl* and *Opg* expression has been examined in bone marrow stromal cells (Rubin et al., 2002a, Gori et al., 2000), and cell cultures exposed to strain showed decreases in *Rankl* expression, whereas *CSF* expression was unaffected (Rubin et al., 2000, Rubin et al., 2002b). Different patterns of fluid flow can either downregulate (Kim et al., 2006) or upregulate (Liu et al., 2010) the *Rankl*/*Opg* expression ratio. In the periodontium, occlusal trauma, such as hyperocclusion may affect *Rankl* and *Runx2* ratios, but in normally functioning animals expression levels remain steady (Claudino et al., 2010). In the present study, a trend toward higher *Rankl* expression was noted in the bone near molars relative to the diastema, but the gene expression patterns did not differ to the extent observed in the mouse hyperocclusion study. Overall, the present data indicate that transitions in bone structure are achieved in association with changes in tooth eruption and functional conditions despite similarities in gene expression.

Acknowledgments

Supported by NIH/NIDCR DE015815. Special thanks to the laboratories of Dr. Martha Somerman and Dr. Susan Herring for making these studies possible.

References

Bosch P, Pratt SL, Stice SL. Isolation, characterization, gene modification, and nuclear reprogramming of porcine mesenchymal stem cells. Biol Reprod. 2006; 74:46–57. [PubMed: 16162872]

Burr DB. Remodeling and the repair of fatigue damage. Calcif Tissue Int. 1993; 53:S75–S81. [PubMed: 8275384]

Chen J, Mcculloch CAG, Sodek J. Bone sialoprotein in developing porcine dental tissues: cellular expression and comparison of tissue localization with osteopontin and osteonectin. Archs Oral Biol. 1993; 38:214–249.

Claudino M, Garlet TP, Cardoso CRB, Assis GFD, Taga R, Cunha FQ, Silva JOS, Garlet GP. Down-regulation of expression of osteoblast and osteocyte markers in periodontal tissues associated with the spontaneous alveolar bone loss of interleukin-10 knockout mice. Eur J Oral Sci. 2010; 118:19–28. [PubMed: 20156261]

Deguchi T, Takano-Yamamoto T, Yabuuchi T, Ando R, Roberts WE, Garetto LP. Histomorphometric evaluation of alveolar bone turnover between the maxilla and the mandible during experimental tooth movement in dogs. Am J Orthod Dentofac Orthop. 2008; 133:889–97.

Dixon, AD.; Hoyte, DAN.; Ronning, O. Fundamentals of Craniofacial Growth. CRC Press; New York: 1997.

Ducy P. Cbfa1: A molecular switch in osteoblast biology. Dev Dyn. 2000; 219:461–471. [PubMed: 11084646]

Ducy P, Zhang R, Geoffroy V, Ridall AL, Karsenty G. Osf2/Cbfa1: A transcriptional activator of osteoblast differentiation. Cell. 1997; 89:747–754. [PubMed: 9182762]

Fazzalari NC, Kuliwaba JS, Atkins GJ, Forwood MR, Findlay DM. The ratio of messenger RNA levels of receptor activator of nuclear factor kB ligand to osteoprotegerin correlates with bone remodeling indices in normal human cancellous bone but not in osteoarthritis. J Bone Min Res. 2001; 16:1015–1027.

Franceschi RT, Xiao G. Regulation of the osteoblast-specific transcription factor, Runx2: responsiveness to multiple signal transduction pathways. J Cell Biochem. 2003; 88:446–454. [PubMed: 12532321]

Francillon-Viellot, H.; De Buffrénil, V.; Castanet, J.; Géraudie, J.; Meunier, FJ.; Sire, JY.; Zylberberg, L.; De Ricqlés, A. Microstructure and mineralization of vertebrate skeletal tissues. In: Carter, JG., editor. Skeletal Biomineralization: Patterns, Processes and Evolutionary trends. Vol. 1. Van Nostrand Reinhold; New York: 1990.

Frost HM. Bone “Mass” and the “Mechanostat”: a proposal. Anat Rec. 1987; 219:1–9. [PubMed: 3688455]

Gori F, Hofbauer LC, Dunstan CR, Spelsberg TC, Khosla S, Riggs BL. The Expression of Osteoprotegerin and RANK Ligand and the Support of Osteoclast Formation by Stromal-Osteoblast Lineage Cells Is Developmentally Regulated. Endocrinology. 2000; 141:4768–4776. [PubMed: 11108292]

Heinrich J, Bsoul S, Barnes J, Woodruff K, Abboud S. CSF-1, RANKL and OPG regulate osteoclastogenesis during murine tooth eruption. Archs Oral Biol. 2005; 50:897–908.

Huja SS, Fernandez SA, Hill KJ, Li Y. Remodeling dynamics in the alveolar process in skeletally mature dogs. Anat Rec Part A: Discoveries in Molecular, Cellular, and Evol Biol. 2006; 288A: 1243–1249.

Katagiri T, Takahashi N. Regulatory mechanisms of osteoblast and osteoclast differentiation. Oral Diseases. 2002; 8:147–159. [PubMed: 12108759]

Kim CH, You L, Yellowley CE, Jacobs CR. Oscillatory fluid flow-induced shear stress decreases osteoclastogenesis through RANKL and OPG signaling. Bone. 2006; 39:1043–1047. [PubMed: 16860618]

Komori T. Regulation of bone development and extracellular matrix protein genes by Runx2. Cell Tissue Res. 2010; 339:189–195. [PubMed: 19649655]

Kon T, Cho TJ, Aizawa T, Yamazaki M, Nooh N, Graves D, Gerstenfeld LC, Einhorn TA. Expression of osteoprotegerin, receptor activator of NF-kB ligand (osteoprotegerin ligand) and related proinflammatory cytokines during fracture healing. J Bone Min Res. 2001; 16:1004–1014.

Liu C, Zhao Y, Cheung WY, Gandhi R, Wang L, You L. Effects of cyclic hydraulic pressure on osteocytes. Bone. 2010; 46:1449–56. [PubMed: 20149907]

Liu D, Yao S, Pan F, Wise GE. Chronology and regulation of gene expression of RANKL in the rat dental follicle. Eur J Oral Sci. 2005; 113:404–409. [PubMed: 16202028]

Marks SC, Cahill DR. Ultrastructure of alveolar bone during tooth eruption in the dog. Amer J Anat. 1986; 177:427–428. [PubMed: 3799493]

Mavropoulos A, Kiliaridis S, Bresin A, Ammann P. Effect of different masticatory functional and mechanical demands on the structural adaptation of the mandibular alveolar bone in young growing rats. Bone. 2004; 35:191. [PubMed: 15207756]

Ogasawara T, Yoshimine Y, Kiyoshima T, Kobayashi I, Matsuo K, Akamine A, Sakai H. *In situ* expression of RANKL, RANK, osteoprotegerin and cytokines in osteoclasts of rat periodontal tissue. J Periodontal Res. 2004; 39:42–49. [PubMed: 14687227]

Ogata Y. Bone sialoprotein and its transcriptional regulatory mechanism. J Periodont Res. 2008; 43:127–135. [PubMed: 18302613]

Par Azeredo RA, Watanabe IS, Beigno MIM, Lemos JLR, Liberti EA. The arrangement of the trabecular bone in the vestibular surface of the human fetus mandible. A scanning electron microscopy study. Morphologie. 2000; 84:19–24. [PubMed: 11244928]

Perinpanayagam H, Martin T, Mithal V, Dahman M, Marzec N, Lampasso J, Dziak R. Alveolar bone osteoblast differentiation and Runx2/Cbfa1 expression. Archs Oral Biol. 2006; 51:406–415.

Pilipili CM, Goret-Nicaise M, Dhem A. Microradiographic aspects of the growing mandibular body during permanent premolar eruption in the dog. Eur J Oral Sci. 1998; 106:429–436. [PubMed: 9541260]

Powell K, Atkinson PJ, Woodhead C. Cortical bone structure of the pig mandible. Archs Oral Biol. 1973; 18:171–180.

Rubin J, Ackert-Bicknell CL, Zhu L, Fan X, Murphy TC, Nanes MS, Marcus R, Holloway L, Beamer WG, Rosen CJ. IGF-I regulates osteoprotegerin (OPG) and receptor activator of nuclear factor-{kappa}B ligand *in vitro* and OPG *in vivo*. J Clin Endocrinol Metab. 2002a; 87:4273–4279. [PubMed: 12213884]

Rubin J, Murphy T, Nanes MS, Fan X. Mechanical strain inhibits expression of osteoclast differentiation factor by murine stromal cells. Am J Physiol Cell Physiol. 2000; 278:C1126–C1132. [PubMed: 10837340]

Rubin J, Murphy TC, Fan X, Goldschmidt M, Taylor W. Activation of extracellular signal-regulated kinase is involved in mechanical strain inhibition of RANKL expression in bone stromal cells. J Bone Min Res. 2002b; 17:1452–1460.

Saffar JL, Lasfargues JJ, Cherruau M. Alveolar bone and the alveolar process: the socket that is never stable. Periodontology 2000. 1997; 13:76–90. [PubMed: 9567924]

Taylor D, Lee TC. Microdamage and mechanical behaviour: predicting failure and remodelling in compact bone. J Anat. 2003; 203:203–211. [PubMed: 12924820]

Terespolsky MS, Brin I, Harari D, Steigman S. The effect of functional occlusal forces on orthodontic tooth movement and tissue recovery in rats. Amer J Orthodont Dentofacial Orthoped. 2002; 121:620–628.

Van Wesenbeeck L, Odgren PR, Mackay CA, D'angelo M, Safadi FF, Popoff SN, Van Hul W, Marks SC Jr. The osteopetrotic mutation toothless (tl) is a loss-of-function frameshift mutation in the rat Csf1 gene: Evidence of a crucial role for CSF-1 in osteoclastogenesis and endochondral ossification. PNAS. 2002; 99:14303–14308. [PubMed: 12379742]

Verna C, Dalstra M, Lee TC, Cattaneo PM, Melsen B. Microcracks in the alveolar bone following orthodontic tooth movement: a morphological and morphometric study. Eur J Orthodont. 2004; 26:459–467.

Vignery A, Baron R. Dynamic histomorphometry of alveolar bone remodeling in the adult rat. Anat Rec. 1980; 196:191–200. [PubMed: 7416512]

Walker CG, Ito Y, Dangaria S, Luan X, Diekwisch TGH. RANKL, osteopontin, and osteoclast homeostasis in a hyperocclusion mouse model. Eur J Oral Sci. 2008; 116:312–318. [PubMed: 18705798]

Wise GE, Frazier-Bowers S, D'souza RN. Cellular, molecular, and genetic determinants of tooth eruption. Crit Rev Oral Biol Med. 2002; 13:323–334. [PubMed: 12191959]

Wise GE, Huang H, Que BG. Gene expression of potential tooth eruption molecules in the dental follicle of the mouse. Eur J Oral Sci. 1999; 107:482–486. [PubMed: 10625108]

Wise GE, Yao S, Odgren PR, Pan F. CSF-1 Regulation of Osteoclastogenesis for Tooth Eruption. J Dent Res. 2005; 84:837–841. [PubMed: 16109994]

Yasuda H, Shima N, Nakagawa N, Yamaguchi K, Kinosaki M, Goto M, Mochizuki SI, Tsuda E, Morinaga T, Udagawa N, Takahashi N, Suda T, Higashio K. A novel molecular mechanism modulating osteoclast differentiation and function. Bone. 1999; 25:109–113. [PubMed: 10423033]

Yasuda H, Shima N, Nakagawa N, Yamaguchi K, Kinosaki M, Mochizuki S, Tomoyasu A, Yano K, Goto M, Murakami A, Tsuda E, Moringa T, Higashio K, Udagawa N, Takahashi N, Suda T. Osteoclast differentiation factor is a ligand for osteoprotegerin/osteoclastogenesis-inhibitory factor and is identical to TRANCE/RANKL. PNAS. 1998; 95:3597–3602. [PubMed: 9520411]

Yeh K, Popowics T, Rafferty K, Herring S, Egbert M. The effects of tooth extraction on alveolar bone biomechanics in the miniature pig, *Sus scrofa*. Archs Oral Biol. 2010; 55:663–9.

Yeh K-D, Popowics T. The impact of occlusal function on structural adaptation in alveolar bone of the growing pig, *Sus Scrofa*. Archs Oral Biol. 2010 in press. 10.1016/j.archoralbio.2010.08.013

Zeng L, Rahrmann E, Hu Q, Lund T, Sandqist L, Felton M, O'brien TD, Zhang J, Verfaillie C. Multipotent adult progenitor cells from swine bone marrow. Stem Cells. 2006; 24:2355–66. [PubMed: 16931778]

Zhang S, Xiao Z, Luo J, He N, Mahlios J, Quarles LD. Dose-dependent effects of Runx2 on bone development. J Bone Min Res. 2009; 24:1889–1904.

Zou X, Li H, Chen L, Baatrup A, Bünger C, Lind M. Stimulation of porcine bone marrow stromal cells by hyaluronan, dexamethasone and rhBMP-2. Biomaterials. 2004; 25:5375–5385. [PubMed: 15130722]

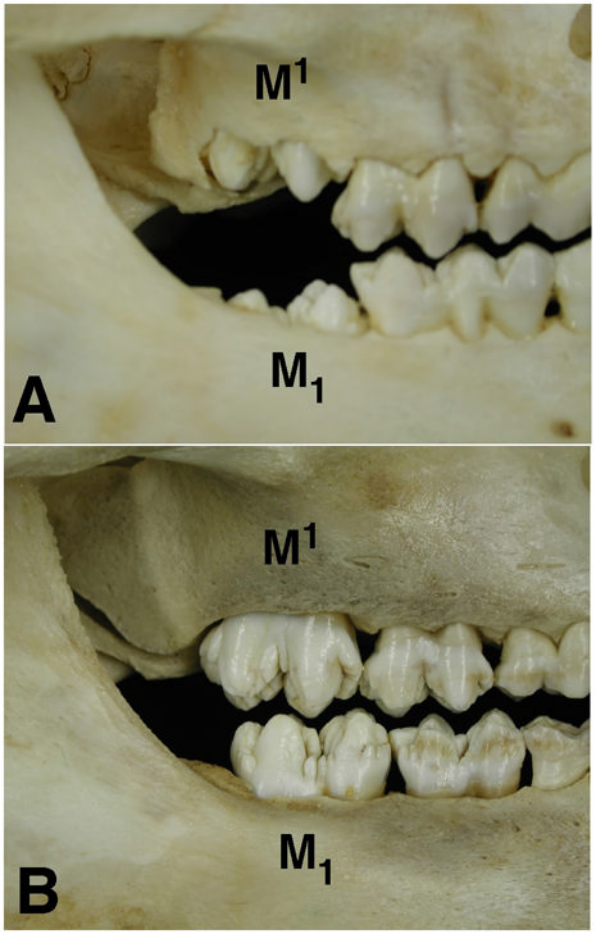

Figure 1.

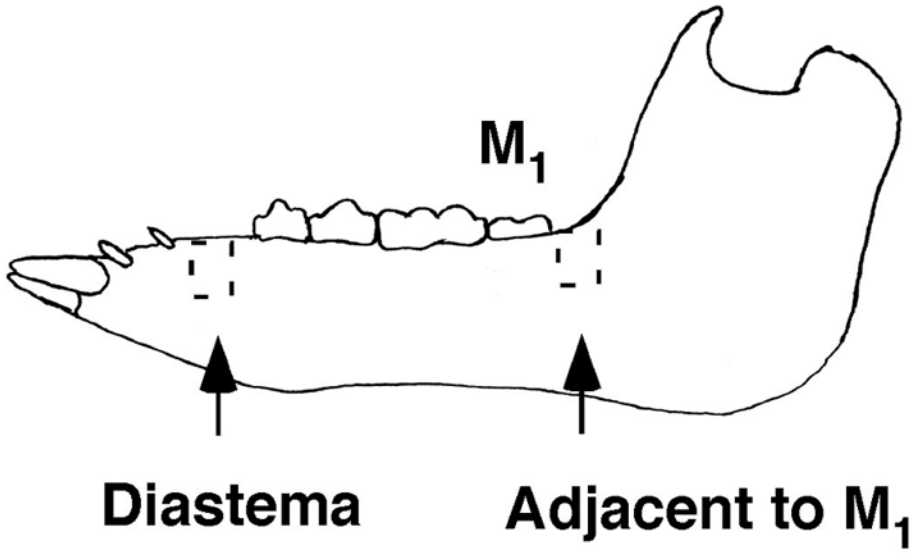

Figure 2.

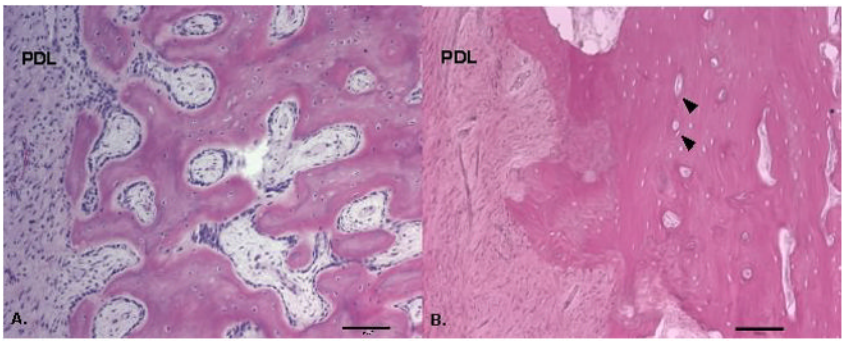

Figure 3.

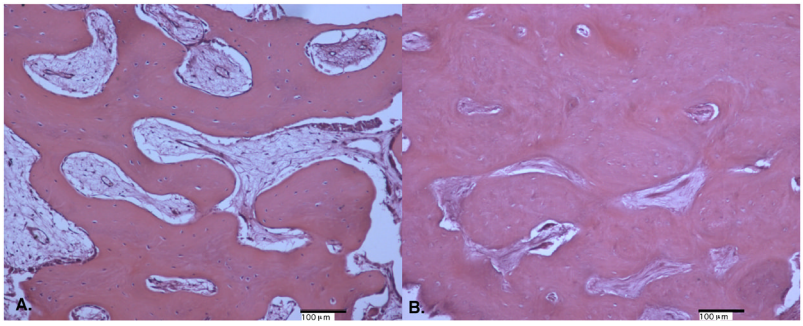

Figure 4.

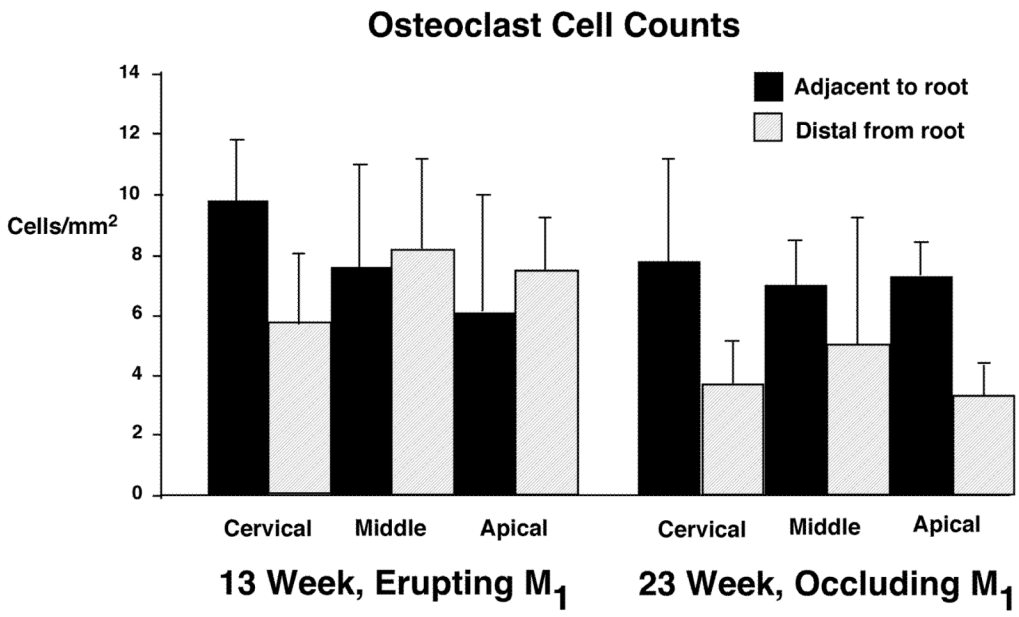

Figure 5.

Table 1

Primer sequences for *Sus scrota* specific genes.

	GenBank accession number	Forward primer (5′ to 3′)	Reverse primer (5′ to 3′)
Rankl	AY60682	TGTGAGACTACTAAGCGG	GCAGGTTCCAGCATGA
Opg	EF543195	GGGGCTCCTTCTAACT	CTCCGCAAGAAGTCCA
Csf-1	AJ583506	TCGTGCCAAATTGCCT	CGTCTCATAGAAAGTTCGGA
Bsp	L10363	ACGAAGGCATGAATTGT	ACGGGTAGGTATCGTGA
Runx2	EU668154	CAAAGCCAGAGCGGAC	AATTTGGATTTAATAGCGTGC
Gapdh	AF017079	GATCGTCAGCAATGCC	CCGGTAGAAGCAGGGA

Table 2

Target gene expression relative to GAPDH from bone samples from the mandibular diastema and distal to the lower first molar.

Pig Number	Age	Location	RANKL	CSF-1	OPG	BSP	RUNX2
4425	13 wk	diastema	0.13 ± 0.003	0.63 ± 0.04	24.68 ± 40.5	27,808 ± 156	4.19 ± 0.13
5060	13 wk	diastema	0.25 ± 0.02	0.70 ± 0.03	188.32 ± 308	20,378 ± 3640	6.32 ± 0.31
5061	13 wk	diastema	0.22 ± 0.03	0.49 ± 0.07	7.17 ± 8.7	20,538 ± 1612	3.61 ± 0.58
Mean	13 wk	diastema	0.20 ± 0.06	0.61 ± 0.11		22,908 ± 4244	4.71 ± 1.42
4501	23 wk	diastema	0.07 ± 0.01	0.23 ± 0.10	18.99 ± 20	11,411 ± 1384	2.14 ± 0.07
5069	23 wk	diastema	0.77 ± 0.04	1.11 ± 0.12	164.07 ± 245.7	211,673 ± 16,868	10.05 ± 0.37
5071	23 wk	diastema	0.34 ± 0.02	0.66 ± 0.02	178.49 ± 222	66,639 ± 851	7.43 ± 0.33
Mean	23 wk	diastema	0.39 ± 0.36	0.67 ± 0.44		96,574 ± 103,432	6.54 ± 4.03
5060	13 wk	M_1 distal	0.61 ± 0.03	1.29 ± 0.16	6800 ± 11,611	44,838 ± 14,325	12.61 ± 2.04
5061	13 wk	M_1 distal	0.43 ± 0.03	0.54 ± 0.06	14,841 ± 20,981	44,796 ± 8683	6.18 ± 0.84
Mean	13 wk	M_1 distal	0.52 ± 0.13	0.92 ± 0.53		44, 817 ± 29	9.39 ± 4.55
4501	23 wk	M_1 distal	0.22 ± 0.03	0.38 ± 0.04	177.25 ± 167.4	27,925 ± 3724	2.15 ± 0.17
5069	23 wk	M_1 distal	0.19 ± 0.03	0.66 ± 0.14	4.49 ± 5.7	3801 ± 334	4.20 ± 1.48
5071	23 wk	M_1 distal	1.10 ± 0.11	1.50 ± 0.25	66.20 ± 61.9	52,224 ± 4721	12.38 ± 1.33
Mean	23 wk	M_1 distal	0.50 ± 0.52	0.84 ± 0.58		27, 983 ± 24,211	6.24 ± 5.41